inorganics

MDPI

Article

Growth, Spectroscopic Characterization and Continuous-Wave Laser Operation of Er,Yb:$GdMgB_5O_{10}$Crystal

Konstantin N. Gorbachenya [1], Elena A. Volkova [2,*], Victor V. Maltsev [2,*], Victor E. Kisel [1], Diana D. Mitina [2], Elizaveta V. Koporulina [2], Nikolai N. Kuzmin [3], Ekaterina I. Marchenko [2] and Vladimir L. Kosorukov [2]

[1] Center for Optical Materials and Technologies, Belarusian National Technical University, Nezavisimosti Ave., 65, 220013 Minsk, Belarus; gorby@bntu.by (K.N.G.)
[2] Department of Crystallography and Crystal Chemistry, Faculty of Geology, Moscow State University, 119234 Moscow, Russia; e_koporulina@mail.ru (E.V.K.)
[3] Institute of Spectroscopy, Russian Academy of Sciences, 108840 Moscow, Russia
* Correspondence: volkova@geol.msu.ru (E.A.V.); maltsev@geol.msu.ru (V.V.M.)

Abstract: A transparent Er^{3+},Yb^{3+}:$GdMgB_5O_{10}$ single crystal with dimensions up to 24 × 15 × 12 mm was grown successfully by the high-temperature solution growth on dipped seeds technique from $K_2Mo_3O_{10}$-based solvent. The grown crystal was characterized using PXRD, DSC and ATR techniques. Differential scanning calorimetry measurements and SEM analysis of the heat-treated solids revealed Er,Yb:$GdMgB_5O_{10}$ to be an incongruent melting compound with an onset point of 1087 °C. The absorption edge of the Er,Yb:GMBO sample is located in the region of 245 nm, which approximates a value of 4.8 eV. Absorption and emission spectra, and luminescence kinetics, were studied. The energy transfer efficiency from ytterbium to erbium ions was determined. The laser operation in continuous-wave mode was realized and output characteristics were measured. The maximal output power of 0.15 W with a slope efficiency of 11% was obtained at 1568 nm.

Keywords: erbium; ytterbium; pentaborate crystal; growth; electronic band; differential scanning calorimetry; spectroscopy; laser operation

Citation: Gorbachenya, K.N.; Volkova, E.A.; Maltsev, V.V.; Kisel, V.E.; Mitina, D.D.; Koporulina, E.V.; Kuzmin, N.N.; Marchenko, E.I.; Kosorukov, V.L. Growth, Spectroscopic Characterization and Continuous-Wave Laser Operation of Er,Yb:$GdMgB_5O_{10}$Crystal. *Inorganics* **2024**, *12*, 240. https://doi.org/10.3390/inorganics12090240

Academic Editor: Binbin Chen

Received: 23 July 2024
Revised: 26 August 2024
Accepted: 28 August 2024
Published: 31 August 2024

1. Introduction

Borate compounds have been extensively studied over the past few decades due to their remarkable structural flexibility and potential applications as laser, nonlinear, scintillation, magnetic and phosphor materials, etc., [1]. The variety of functional properties of borates is based on the diversity of their structural types: boron atoms can be bonded with three or four oxygen atoms, forming planar/non-planar triangular BO_3 or tetrahedral BO_4 fundamental structural units, respectively. These B-O building groups can be connected to each other by common corners or edges, forming different B-O clusters [2]. Nowadays, rare-earth metal borates are very attractive objects for the research community because of their nonlinear optical and laser applications.

Laser radiation in the 1.5–1.6 μm spectral range is extensively used in range finding, optical locating and telecommunications applications, mainly because of its eye safety, weak absorption in the atmosphere and low dispersion and absorption of quartz fibers. This radiation can be obtained using solid-state lasers based on gain media doped with trivalent erbium ions (transition $^4I_{13/2} \rightarrow {}^4I_{15/2}$). However, the main disadvantage of the Er^{3+} ions is low absorption in the spectral range of InGaAs laser diode emissions (near 1 μm), which limits pumping efficiency. Ytterbium ions are a good sensitizer due to the broad absorption band near 1 μm and the large overlap between Yb^{3+} emissions and Er^{3+} absorption, which allows for resonant energy transfer from ytterbium to erbium ions [3].

Recently, the spectroscopic and laser properties of different gain media have been investigated. Among them, phosphate glasses co-doped with Er,Yb ions are the most widely used, since Er,Yb-phosphate glasses are characterized by spectroscopic properties

suitable for efficient laser operation (energy transfer from Yb^{3+} to Er^{3+} ions of 90% with a long lifetime of the erbium upper laser level $^4I_{13/2}$ of 7–8 ms and a short lifetime of the $^4I_{11/2}$ energy level of 2–3 μs) [4]. However, phosphate glass exhibits poor thermo-mechanical properties (a thermal conductivity of 0.85 $W \times m^{-1} \times K^{-1}$) [5], which limits the average output power of Er,Yb:glass lasers in continuous-wave and Q-switched regimes of operation due to the thermal effects.

Crystalline laser hosts are characterized by significantly higher thermal conductivity values than glasses [6,7]. Currently, many crystalline hosts have been investigated for Er,Yb lasers—aluminates, silicates, vanadates, and tungstates [8,9]—but spectroscopic properties of these crystals do not fully meet the requirements for achieving an efficient laser operation. Nowadays, oxoborate crystals are the most important Er,Yb-codoped crystalline laser materials because they possess not only high thermal conductivity but also the necessary spectroscopic properties mentioned above [10,11]. The most efficient laser operation in continuous-wave mode has been demonstrated for huntite-type Er,Yb:$RAl_3(BO_3)_4$ (R = Y, Gd, Lu) [12–14] and pentaborate Er,Yb:$RMgB_5O_{10}$ [15–18] (R = Y, Gd, La) crystals. The pentaborate crystals demonstrate relatively high thermal conductivity and good spectroscopic properties [16]. The highest output power of 0.61 W and slope efficiency of 23% was realized for Er,Yb:$LaMgB_5O_{10}$ [18]. We have recently exhibited a continuous-wave Er,Yb:$YMgB_5O_{10}$ laser with an output power of 0.2 W at 1570 nm [15]. $GdMgB_5O_{10}$ (GMBO) crystal also proved to be a good choice for both Er,Yb-codoping and single Yb-doping. The maximal output power of 0.22 W with a slope efficiency of 14% at 1569 nm was demonstrated for Er,Yb:$GdMgB_5O_{10}$ [19], while up to 5.35 W and 56% of maximal output power and slope efficiency, respectively, were demonstrated at 1060.8 nm for Yb:$GdMgB_5O_{10}$ [20].

In the present work, a comprehensive characterization including growth technique, thermal stability, IR spectroscopy, bandgap transmission spectra, and spectroscopic and laser properties of as-grown Er,Yb:$GdMgB_5O_{10}$ single crystals was carried out.

2. Results and Discussion

2.1. Growth Technique and Structure Characterization

A transparent macrodefect-free Er,Yb-codoped $GdMgB_5O_{10}$ single crystal with a size of 24 × 15 × 12 mm was grown by the high-temperature solution growth on dipped seeds (HT-SGDS) technique (Figure 1). The saturation temperature value obtained was about ~950 °C.

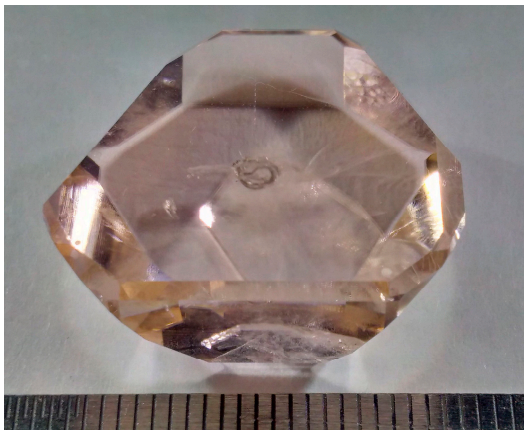

Figure 1. As-grown Er,Yb:$GdMgB_5O_{10}$ single crystal.

The Le Bail fitting was performed to confirm the structural similarity of Er,Yb:GMBO to rare-earth magnesium pentaborates. To perform the Le Bail method, the crystal symmetry and lattice parameters for $GdMgB_5O_{10}$ (database code: ICSD 157426) were used as input data. Powder X-ray diffraction (PXRD) refinements showed good agreement with the

theoretical profile. Nevertheless, pattern matching revealed an impurity phase, SiO_2, which appeared after grinding in the agate mortar (Figure 2).

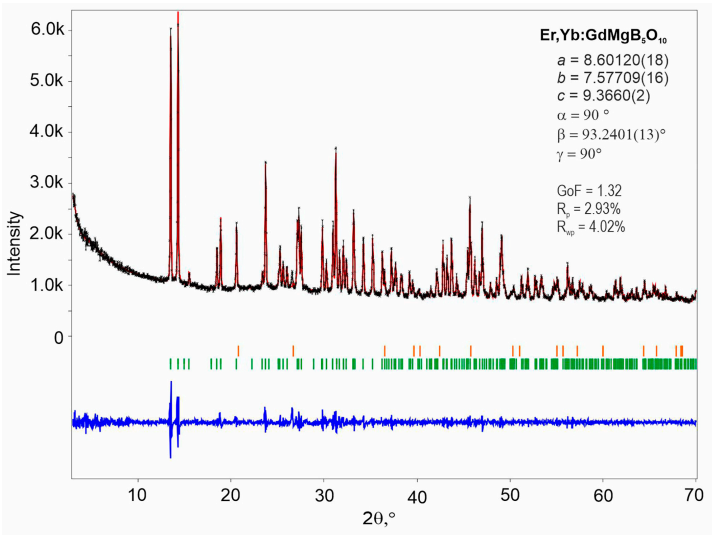

Figure 2. Diffraction profiles showing observed (black crosses) and calculated (red continuous line) profiles, and the difference curve (blue continuous line) between observed and calculated spectra. Green and orange vertical markers represent Bragg reflections corresponding to the main phase of $GdMgB_5O_{10}$ (ICSD 157426) and the impurity phase of SiO_2 (COD 1526860), respectively.

The thermal behavior of the Er,Yb:GMBO compound was determined by differential scanning calorimetry (DSC). A fragment of calorimetric data in the temperature range 600–1200 °C is shown in Figure 3. The heating curve is characterized by a sharp endothermic peak with an onset temperature of ~1087 °C. However, no exothermic peak is observed on the cooling curve, indicating the incongruent melting of the compound under investigation.

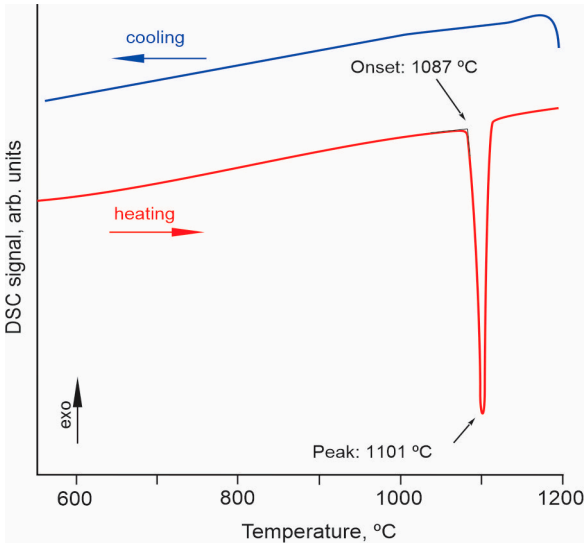

Figure 3. DSC curves of Er,Yb:$GdMgB_5O_{10}$ crystal in the temperature range of 600–1200 °C.

Similar thermal behavior has been previously described for $TmMgB_5O_{10}$ and $YMgB_5O_{10}$, which undergo incongruent melting to form RBO_3 and $Mg_2B_2O_{10}$ phases [21]. Spontaneous Er,Yb:GMBO crystals from the crystallized (after cooling) molten bath were annealed in an alundum crucible at 1050 °C and characterized using the SEM/EDXS technique. The residue in the crucible after heat treatment was a white, translucent, dense mass containing

mostly partially melted pentaborate crystals (Figure 4). SEM/EDXS data revealed the existence of two phases other than Er,Yb:GMBO.

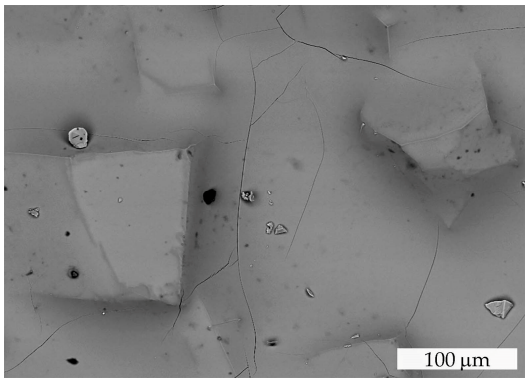

Figure 4. SEM image of the Er,Yb:GMBO spontaneous crystals heat-treated at 1050 °C .

The distribution patterns of the elements in the X-ray characteristic radiation show that the bright phase formed is enriched in the rare-earth component and the darker one is enriched in magnesium (Figure 5). It is impossible to determine the distribution of boron in the newly formed phases from the SEM data, but it can be assumed that the first phase is represented by rare-earth orthoborate RBO_3 (due to the high stability of this phase in a wide temperature range), and the secondby the magnesium phase. Considering previous studies on the thermal properties of Tm and YMg pentaborates, the thermally induced process can be described by the following reaction:

$$2RMgB_5O_{10} \rightarrow 2RBO_3 + Mg_2B_2O_5 + 3B_2O_3, \text{ where } R = \text{Er, Yb, and Gd.}$$

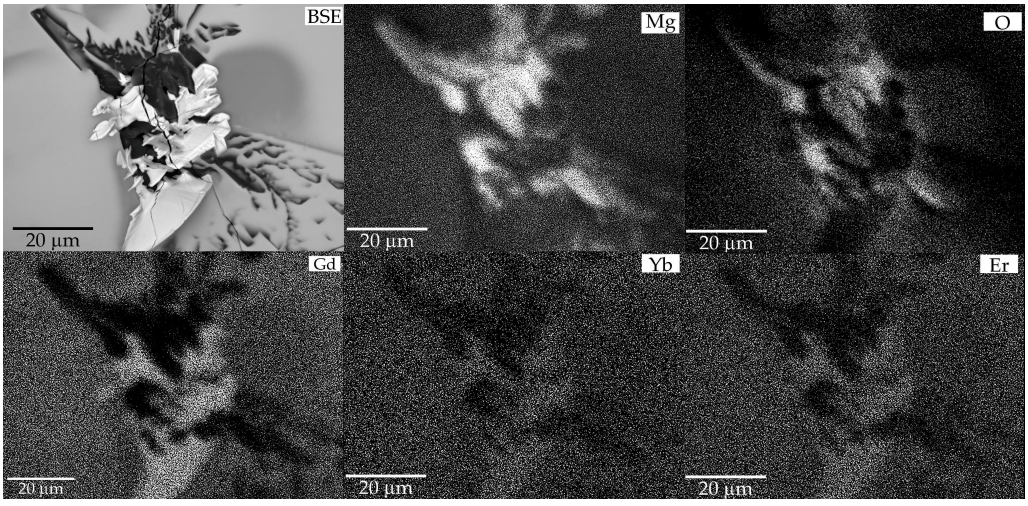

Figure 5. SEM/EDXS patterns of the decomposition products after annealing Er,Yb:GMBO spontaneous crystals.

Figure 6 shows the ATR spectrum of Er,Yb:$GdMgB_5O_{10}$. Factor-group analysis for $RMgB_5O_{10}$ compounds was performed in $RMgB_5O_{10}$ compounds [21]. According to it, the $GdMgB_5O_{10}$ compound exhibits 201 optically active modes, of which 99 are IR active. The ATR spectrum contains 40 modes. The smaller number of observed modes is explained by the fact that they cannot be resolved due to the large number of lattice vibrations with close frequencies, and that below 250 cm^{-1} there is strong absorption, associated with intense modes [21].

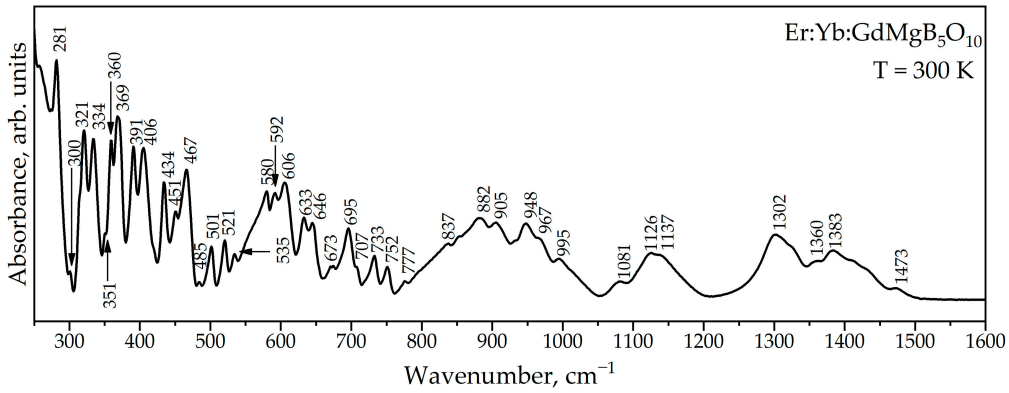

Figure 6. ATR spectrum of Er:Yb:$GdMgB_5O_{10}$.

Figure 7a demonstrates the transmission spectrum of Er,Yb:$GdMgB_5O_{10}$ crystal in the range of 220–300 nm. The absorption edge of the Er,Yb:GMBO sample is located in the region of 245 nm, which is about 30 nm larger than for $YMgB_5O_{10}$ [22]. The optical band gap (E_g) obtained from transmission spectra approximates a value of 4.8 eV (Figure 7b) according to methodology from [23]. The formulas for indirect gap semiconductors were used to calculate the band gap.

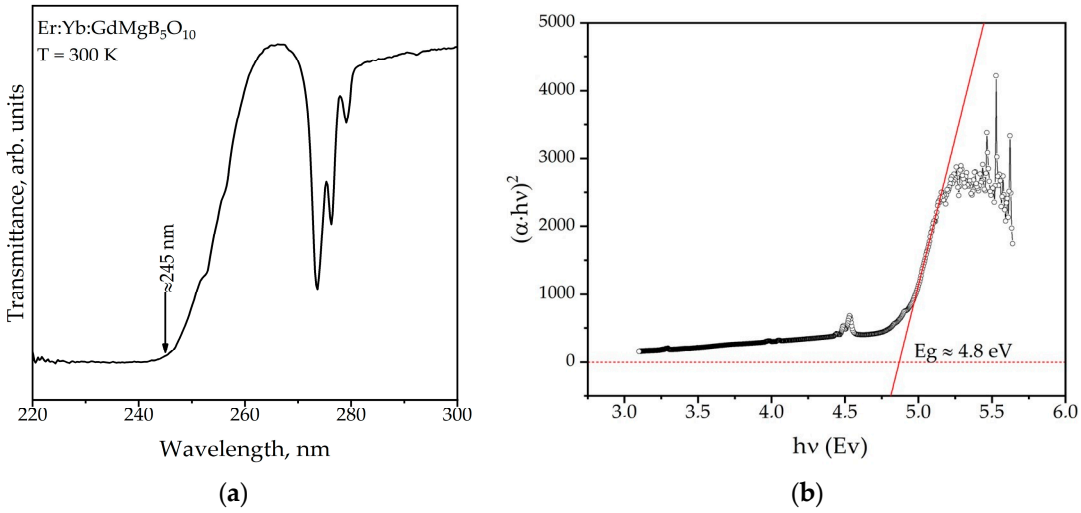

Figure 7. Transmission spectrum (**a**) and related Tauc plot (**b**) of the Er:Yb:$GdMgB_5O_{10}$ crystal.

2.2. Spectroscopy

The room-temperature polarized absorption cross-section spectra of the Er,Yb:GMBO crystal in the 850–1100 nm spectral range are shown in Figure 8. The peak absorption cross-sections around 976 nm (the wavelength is close to the emission wavelengths of commercial InGaAs laser diodes) corresponding to the $^2F_{7/2} \rightarrow {}^2F_{5/2}$ transitions of Yb^{3+} ions are about 1.5×10^{-20} cm^2 for $E//N_g$polarization. Therefore, the polarization of the pump beam that matches the N_g axis of the crystal is preferred.The FWHM near 976 nm is ~2 nm, which imposes additional requirements for the wavelength stabilization of laser diodes.

Figure 9 shows the polarized absorption cross-section of the Er,Yb:GMBO crystal at room temperature near 1.5 µm. Structured spectra with several narrow bands related to the $^4I_{15/2} \rightarrow {}^4I_{13/2}$transition of Er^{3+} ions are observed in the 1400–1650 nm spectral range. Multiple peaks in the absorption cross-section spectra correspond to transitions between the stark sublevels of the lower and upper multiplets. One can note the similarity with the data presented for Er,Yb:YMBO in [15].The maximum absorption cross-section does not exceed 1.1×10^{-20} cm^2 at the wavelength of 1530 nm.

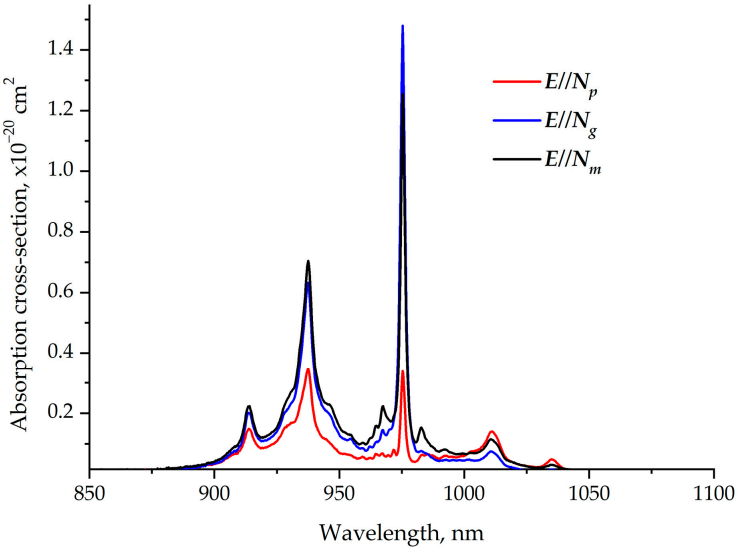

Figure 8. Polarized room-temperature absorption cross-section spectra of Er,Yb:GMBO crystal near 1 μm.

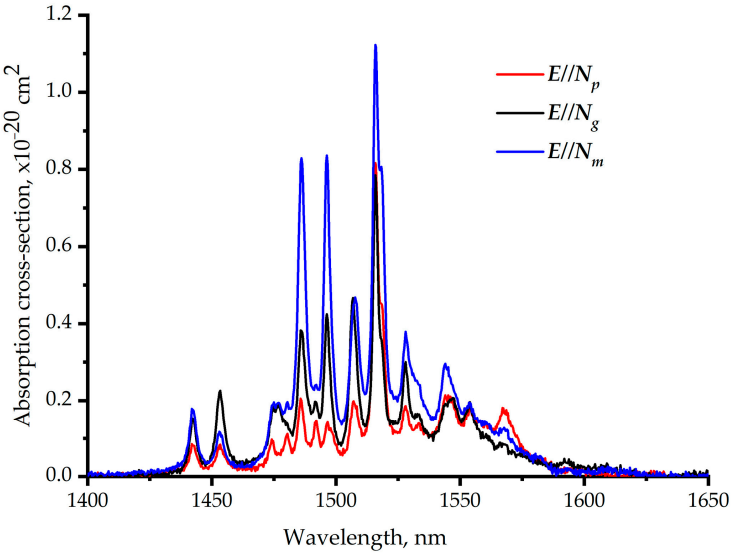

Figure 9. Polarized room-temperature absorption cross-section spectra of the Er,Yb:GMBO crystal near 1.5 μm.

The decay curve of the 1.5 μm emission is shown in Figure 10. It was approximated by a single exponential function, and the $^4I_{13/2}$ energy level of Er^{3+} was found to be 430 ± 20 μs. We can note that the influence of reabsorption is not significant for the $^4I_{13/2}$ erbium energy level measurements. The emission lifetime was calculated using the Judd–Ofelt method and amounted to 6.30 ms (the corresponding data are given in [16]). Thus, the quantum yield of luminescence does not exceed 7%, which is comparable to values demonstrated previously for other oxoborate crystals with high phonon energy [13].

To calculate energy transfer efficiency from ytterbium to erbium according to Equation (1), the lifetime of the $^2F_{5/2}$energy level of Yb^{3+} in Yb single-doped crystal and the Er,Yb-codoped one was measured. The dependence of the measured $^2F_{5/2}$-energy-level lifetime of Yb^{3+}on ytterbium content using Yb:GMBO powder in glycerin is presented in Figure 11.

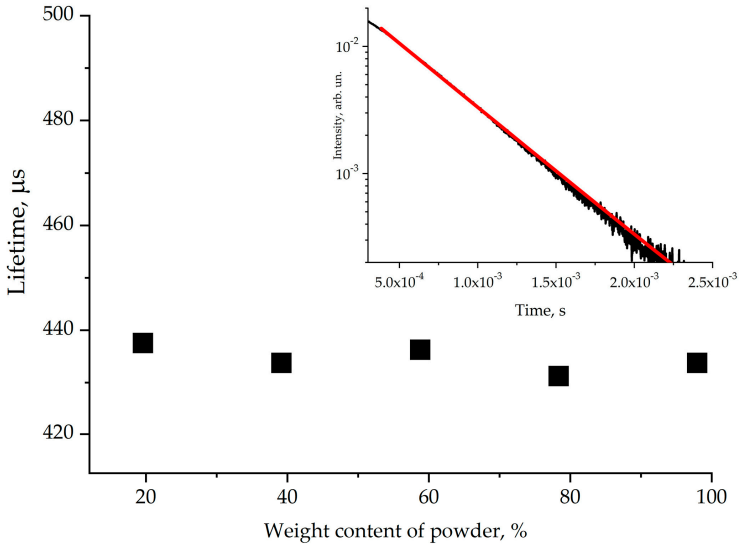

Figure 10. The lifetime of the erbium $^4I_{13/2}$ energy level measured using Er,Yb:GMBO crystalline powder in glycerin. The inset shows luminescence decay kinetics near 1.5 μm.

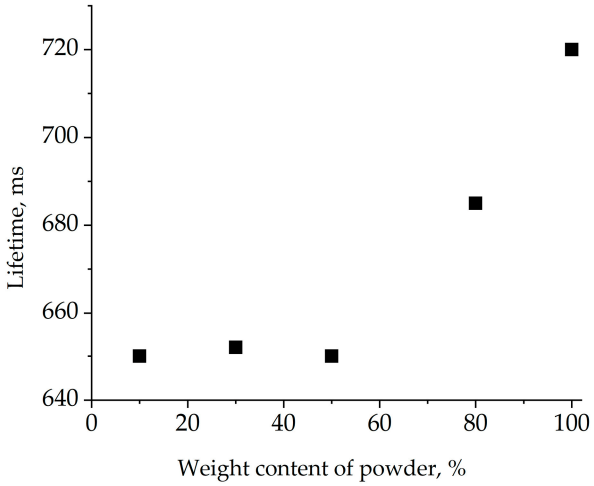

Figure 11. Lifetime of the $^2F_{5/2}$ Yb^{3+} energy level measured using Yb:GMBO crystalline powder in glycerin.

The measured lifetime decreased with decreasing powder content in the suspension. Starting from a certain powder content, the lifetime did not change despite further dilution, suggesting a negligible influence of reabsorption. The lifetime of the $Yb^{3+}{}_2F_{5/2}$ energy level in the Yb(1 at.%):GMBO crystal was 650 ± 30 μs. The measurement of the $Yb^{3+2}F_{5/2}$-energy-level lifetime of Er,Yb:GMBO was similar to above and the $^2F_{5/2}$-energy-level lifetime of Er,Yb:GMBO crystal was determined to be 60 ± 5 μs. Thus, the calculated energy transfer efficiency in the Er,Yb:GMBO crystal doped with 2 at.% Er^{3+} and 11 at.% Yb^{3+} was close to 90%. These results show that the almost all of the absorbed energy may be efficiently transferred from the $^2F_{5/2}$ energy level of the Yb^{3+}ion to the $^4I_{11/2}$energy level of the Er^{3+} ion by a non-radiative resonant energy transfer process. It is also worth noting that the energy transfer efficiency in Er,Yb:GMBO crystals is similar to that of Er,Yb:$RAl_3(BO_3)_4$ and Er,Yb:$YMgB_5O_{10}$ [15].

The stimulated emission cross-section spectra of Er,Yb:GMBO crystal in the 1400–1650 nm range are presented in Figure 12. The emission cross-section is 0.7 × 10^{-20} cm^2at a laser wavelength of 1568 nm for the polarization of $E//N_p$. The inset shows the gain cross-section spectra of the Er,Yb:GMBO crystal for different inversion parameters β ranging from 0.2 to 0.8 in the 1480–1600 nm spectral range for $E//N_p$ polarization.

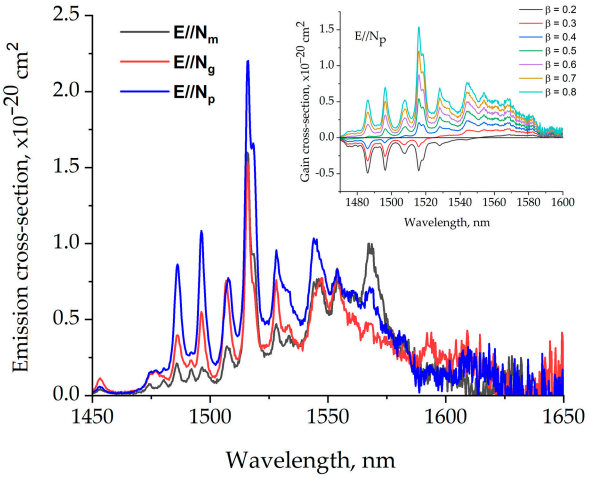

Figure 12. The stimulated emission cross-section spectra of the Er,Yb:GMBO crystal. The inset shows the gain cross-section spectra of the Er,Yb:GMBO crystal.

2.3. Laser Operation

The continuous-wave Er,Yb:GMBO laser operation was realized for output couplers (OCs) with transmissions of 1%, 2% and 5%. The maximal output power and slope efficiency was obtained for OCs with a transmission of 2% at the laser wavelength. The input–output characteristics of a continuous-wave Er,Yb:GMBO laser with a 2% OC is presented in Figure 13. The maximum output power of 0.15 W at 1568 nm with a slope efficiency of 11% was achieved at an absorbed pump power of 3.3 W. Degradation of the output characteristics was observed with increasing incident power, which may be due to the influence of thermal lensing. The laser threshold was approximately 1.8 W of absorbed pump power. The laser radiation was linearly polarized ($E//N_p$). The spatial profile of the output beam was TEM_{00} mode with $M^2 < 1.2$ during all laser operations (inset in Figure 13).

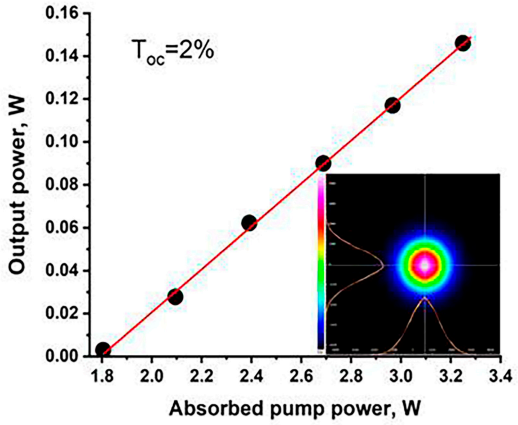

Figure 13. The input–output characteristics of Er,Yb:GMBO laser; the inset shows the spatial profile of the output beam.

3. Materials and Methods

(Er,Yb):$GdMgB_5O_{10}$ bulk crystal was grown by the HT-SGDS technique from $K_2Mo_3O_{10}$ solvent in the temperature range 870–830°C. Previously, experiments on GMBO spontaneous crystallization were carried out to estimate acceptable fluxed melt composition, taking into account the peculiarities of phase formation in other *R*MBO-$K_2Mo_3O_{10}$ systems [24]. Based on the results obtained, a complex system of the composition 20 wt.% Er,Yb:GMBO–80 wt.% $K_2Mo_3O_{10}$ was applied in growth experiments. The $R_2O_3/MgO/B_2O_3$ (where *R* = Yb, Er, Gd) ratio was set according to the pentaborate formula (1:2:5 in molar fractions). Er_2O_3 (99.96%), Yb_2O_3 (99.96%), Gd_2O_3 (99.96%), MgO (A.C.S. grade, by Aldrich), and B_2O_3

(A.C.S. grade, by Alfa Aesar) were used as crystal-forming agents, which were weighed according to the composition of $Er_{0.02}Yb_{0.11}Gd_{0.87}MgB_5O_{10}$. The solvent, $K_2Mo_3O_{10}$, was prepared from a mixture of K_2MoO_4 (A.C.S. grade, Chimkraft, Kaliningrad, Russia) and MoO_3 (A.C.S. grade, Aldrich), compounded in a molar ratio of 1:2.

The starting chemicals were carefull y ground, mixed, and in the 250 mL platinum crucible placed into the furnace at a position that could be adjusted for an optimum temperature gradient. Then, the initial load was heated to a maximum temperature of 100–150 °C above the expected saturation temperature (T_{sat}). After solution homogenization for 24 h, the system was cooled to 5–10 °C above the expected T_{sat}. The saturation point was then precisely confirmed by dipping a trial GMBO seed in the solution and observing the growth/dissolutionprocesses of the crystal faces at different temperatures. Er,Yb:GBMO bulk crystal was obtained using a well-faceted spontaneous crystal. A GBMO seed was dipped into the solution and overheated by 2–3 °C above the fluxed melt saturation temperature to slightly dissolve the outer surface and ensure defect-free nucleation. Subsequently, the temperature was lowered to the T_{sat} in 1 h. During crystal growth, supersaturation was maintained by cooling down from 0.5 to 2 °C per day. At the end, the crystal was extracted and cooled down to room temperature for several days to prevent cracking due to the thermal shock. All experiments were carried out in a vertical tube furnace, equipped with a CrNi alloy resistive heater and a Proterm-100 precision temperature controller connected with a set of Pt-Rh/Pt thermocouples. The temperature in the furnace working zone was kept with a stability of ±0.1°C.

PXRD studies were performed on a Rigaku MiniFlex-600 powder diffractometer (Rigaku Corp., Tokyo, Japan). PXRD data sets were collected in continuous mode at room temperature (CuK_α radiation) in the range of 2θ = 3–70°, and a scan speed of 5° per minute. The PXRD data were analyzed using the model-biased Le Bail fitting with Yana2006 software [25]. Phases were identified using the Match! software package, version 3.8.1.143 [26], the Crystallographic Open Database (COD) and the ICSD inorganic crystal database [27].

The composition and homogeneity of the Er,Yb:GdMB crystal were studied using the analytical scanning electron microscope (SEM) Leo 1420 VP equipped with the energy dispersive X-ray spectrometer (EDXS) INCA 350. Qualitative analysis was performed on the as-grown face. The sample was fixed on a conductive carbon adhesive tape and covered with a thin layer of carbon to prevent charge accumulation on the crystal during interactions with an electron beam. The Er^{3+} and Yb^{3+} distribution coefficient (K_d) was defined as $K_d = C_{cryst}/C_s$, where C_{cryst} is the Er^{3+} and Yb^{3+} content in the crystal and C_s is the nominal concentration of rare-earth oxides in the initial load.

DSC analysis was performed on a STA 449 F5 Jupiter® (Netzsch, Selb, Germany) to investigate the thermal behavior of the Er,Yb:GMBO crystal. DSC measurements were performed in the temperature range of 50–1200 °C at a heating rate of 20 °C/min under argon gas flow. PtRh20 crucibles with a volume of 85 µL were used for the experiments. The melting point was determined based on the onset temperature of the melting process, with an estimated uncertainty of ±5 °C. To further investigate the thermal behavior, crystals obtained were heat-treated in the range of 1050 °C. The products after annealing were analyzed using the SEM/EDXS method to identify any changes in the phase composition.

Spontaneous Er:Yb:$GdMgB_5O_{10}$ crystals were ground into powder in a corundum mortar to record attenuated total reflection (ATR) spectra. The measurements were carried out on a Fourier spectrometer Bruker IFS 125HR at room temperature in the spectral range 50–2000 cm^{-1} with a resolution of 2 cm^{-1}. In this case, a Mylar beamsplitter and a DTGS receiver were used in the far-infrared(IR) range (50–700 cm^{-1}). A KBr beamsplitter and a DLaTGS receiver were used in the mid-IR range (400–2000 cm^{-1}). In both cases, the source was a Globar.

Transmission spectra in the ultraviolet (UV) range were recorded on an Ocean Insight OCEAN-HDX-UV-VIS spectrometer at room temperature in the spectral range 200–800 nm

with a resolution of 0.73 nm. A deuterium lamp was used as a source, and a CCD detector served as a receiver. The measurements used a fragment of a small crystal.

Er,Yb:GMBO is a monoclinic crystal, it is optically biaxial and its optical properties are described along the three main optical axes of the N_g, N_m, and N_p indicatrices [28]. For spectroscopic investigations in polarized light, plates oriented along N_g, N_m, and N_p indicatrices were cut from the Er,Yb:GMBO crystal. The polarized absorption spectra were measured at room temperature by using spectrophotometer Agilent Cary 5000. The absorption cross-section spectra were calculated according to (1):

$$\sigma_{abs}(\lambda) = \frac{k_{abs}(\lambda)}{N} \quad (1)$$

where $k_{abs}(\lambda)$ is the absorption coefficient, N is the concentration of ytterbium for near-1 μm spectra or erbium for near-1.5 μm spectra.

For lifetime measurements, a parametric oscillator based on β-$Ba_2B_2O_4$ crystal pumped by a 355 nm Nd:YAG laser (third harmonic) was used as an excitation source. Luminescence of the sample was collected from its surface irradiated with an excitation beam, passed through an MDR-12 monochromator, and recorded by an InGaAs photodiode with a preamplifier coupled to a 500 MHz digital oscilloscope.

The energy transfer efficiency was calculated according to (2) [29]:

$$\eta = \tau(1/\tau - 1/\tau_0) \quad (2)$$

where τ is the ytterbium $^2F_{5/2}$-level lifetime in Er,Yb-codoped crystal, and τ_0 is the ytterbium $^2F_{5/2}$-level lifetime in Yb single-doped crystal. For Yb^{3+} lifetime measurements, luminescence kinetics were registered by using immersed Er,Yb:GMBO fine powder that enables minimizingreabsorption influence [30].

The calculation of the stimulated emission spectra in the range near 1.5 μm (transition $^4I_{13/2} \rightarrow {}^4I_{15/2}$) was performed by using the integral reciprocity method according to (3) [31] and radiative lifetime of the $^4I_{13/2}$energy level obtained from the Judd–Ofelt theory in [17].

$$\sigma_{\mathrm{em}}^{\alpha}(\lambda) = \frac{3\exp(-hc/(kT\lambda))}{8\pi n^2 \tau_{\mathrm{rad}} c \sum_{\gamma} \int \lambda^{-4} \sigma_{\mathrm{abs}}^{\gamma}(\lambda) \exp(-hc/(kT\lambda)) \mathrm{d}\lambda} \sigma_{\mathrm{abs}}^{\alpha}(\lambda) \quad (3)$$

where $\sigma_{em}(\lambda)$ is the stimulated emission cross-section; α, γ denote the polarization of light; h is Planck's constant; c is the speed of light in a vacuum; k is the Boltzmann constant; T is the temperature of the environment; n is the refractive index of the crystal; τ_{rad} is the radiation lifetime of the $^4I_{13/2}$ energy level of erbium ions; and $\sigma_{abs}(\lambda)$ is the absorption cross-section.

The gain cross-section spectra g(λ) were calculated for different inversion parameters β by using the following Equation (3):

$$g(\lambda) = \beta\ \sigma_{em}(\lambda) - (1 - \beta)\sigma_{abs}(\lambda) \quad (4)$$

where $\beta = N_{ex}/N_{tot}$ is the ratio of the population of excited Er^{3+} ion manifolds to the total erbium ion concentration.

The experimental setup provided in Figure 14 was used to study the laser properties in acontinuous-wave mode of operation. A plane–plane N_m-cut Er,Yb:GMBO crystal with a length of 1.5 mm was used as a gain medium. It was coated with anti-reflection coatings at the pump and laser wavelengths and mounted on an aluminum heat sink kept at 20 °C. A continuous-wave fiber-coupled laser diode (Ø 105 μm, NA = 0.22) emitting at a wavelength of 976 nm was used for the longitudinal pumping of the gain medium. The plano–plano cavity with a geometrical cavity length of 4 mm was applied. A single-lens focusing system focused the pump beam into a 120μm spot inside the laser crystal. Three output

couplers with different transmission coefficients at laser wavelengths were used in the laser experiments.

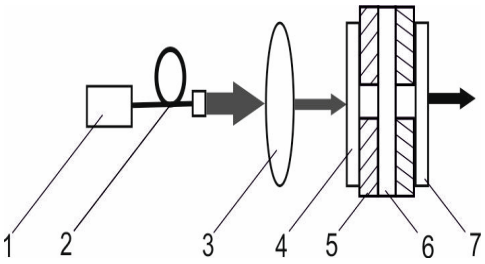

Figure 14. The experimental setup of a continuous-wave diode-pumped Er,Yb:GMBO laser: 1—laser diode; 2—fiber; 3—focusing system; 4—input mirror; 5—copper heat sink; 6—active element; and 7—output coupler.

4. Conclusions

Er^{3+},Yb^{3+}:$GdMgB_5O_{10}$ single crystals with dimensions up to 24 × 15 × 12 mm^3were successfully grown using an HT-SGDS route from a $K_2Mo_3O_{10}$-based flux system. Detailed study of the growth technique and characterization of Er,Yb:$GdMgB_5O_{10}$ single crystal-swere carried out. The spectroscopic properties of as-grown crystals were presented. It was shown that Er,Yb:GMBO crystals are characterized by spectroscopic properties to achieve laser operations. A CW diode-pumped Er,Yb:GMBO laser with an output power of about 150 mW and a slope efficiency of 11% was realized at 1568 nm.

Author Contributions: Software, K.N.G., E.V.K. and E.A.V.; validation, K.N.G., V.E.K., V.V.M., E.A.V., E.V.K., D.D.M., N.N.K., E.I.M. and V.L.K.; investigation, K.N.G., V.E.K., V.V.M., E.A.V., E.V.K., D.D.M., N.N.K., E.I.M. and V.L.K.; resources, K.N.G., V.E.K., E.A.V., E.V.K., V.V.M. and N.N.K.; writing—original draft preparation, K.N.G. and E.A.V.; writing—review and editing, K.N.G. and E.A.V.; visualization, E.A.V. All authors have read and agreed to the published version of the manuscript.

Funding: The work was carried out within the framework of the state budget theme AAAA-A16-116033010121-7 of M.V. Lomonosov MSU. ATR and transmission spectra were obtained with the support of the Ministry of Science and Higher Education of the Russian Federation under the program FFUU-2024-004. This research received no external funding.

Data Availability Statement: The original contributions presented in the study are included in the article, further inquiries can be directed to the corresponding author/s.

Conflicts of Interest: The authors declare no conflicts of interest.

References

1. Mutailipu, M.; Poeppelmeier, K.R.; Pan, S. Borates: A Rich Source for Optical Materials. *Chem. Rev.* **2020**, *121*, 1130–1202. [CrossRef]
2. Leonyuk, N.I.; Maltsev, V.V.; Volkova, E.A. Crystal Chemistry of High-Temperature Borates. *Molecules* **2020**, *25*, 2450. [CrossRef] [PubMed]
3. Hinojosa, S.; Meneses-Nava, M.A.; Barbosa-Garcia, O.; Diaz-Torres, L.A.; Santoyo, M.A.; Mosino, J.F. Energy back transfer, migration and energy transfer (Yb-to-Er and Er-to-Yb) processes in Yb,Er:YAG. *J. Lumin.* **2003**, *102–103*, 694–698. [CrossRef]
4. Karlsson, G.; Laurell, F.; Tellefsen, J.; Denker, B.; Galagan, B.; Osiko, V.; Sverchkov, S. Development and characterization of Yb-Er laser glass for high average power laser diode pumping. *Appl. Phys. B* **2002**, *75*, 41–46. [CrossRef]
5. Taccheo, S.; Sorbello, G.; Laporta, P.; Karlsson, G.; Laurell, F. 230-mW diode-pumped single-frequency Er,Yb laser at 1.5 μm. *IEEE Phot. Techn. Let.* **2001**, *13*, 19–21. [CrossRef]
6. Zagumennyi, A.I.; Lutts, G.B.; Popov, P.A.; Sirota, N.N.; Shcherbakov, I.A. The Thermal conductivity of YAG and YSAG laser crystals. *Laser Phys.* **1993**, *3*, 1064–1065.
7. Krankel, C.; Uvarova, A.; Guguschev, C.; Kalusniak, S.; Hülshoff, L.; Tanaka, H.; Klimm, D. Rare-earth doped mixed sesquioxides for ultrafast lasers. *Opt. Mat. Exp.* **2022**, *12*, 1074–1091. [CrossRef]
8. Schweizer, T.; Jensen, T.; Heumann, E.; Huber, G. Spectroscopic properties and diode-pumped 1.6 μm laser performance in Yb-codoped Er:$Y_3Al_5O_{12}$ and Er:Y_2SiO_5. *Opt. Commun.* **1995**, *118*, 557–561. [CrossRef]

9. Bjurshagen, S.; Brynolfsson, P.; Pasiskevicius, V.; Parreu, I.; Pujol, M.C.; Peña, A.; Aguiló, M.; Díaz, F. Crystal growth, spectroscopic characterization, and eye-safe laser operation of erbium- and ytterbium-codopedKLu$(WO_4)_2$. *Appl. Opt.* **2008**, *47*, 656–665. [CrossRef]
10. Chen, Y.; Lin, Y.; Huang, J.; Gong, X.; Luo, Z.; Huang, Y. Spectroscopic and laser properties of Er^{3+},Yb^{3+}:$LuAl_3(BO_3)_4$ crystal at 1.5-1.6 μm. *Opt. Express* **2010**, *18*, 13700–13707. [CrossRef]
11. Huang, J.; Chen, Y.; Gong, X.; Lin, Y.; Luo, Z.; Huang, Y. Spectral and laser properties of Er,Yb:$Sr_3Lu_2(BO_3)_4$ crystal at 1.5–1.6 μm. *Opt. Express* **2013**, *3*, 1885–1892. [CrossRef]
12. Gorbachenya, K.N.; Kisel, V.E.; Yasukevich, A.S.; Deineka, R.V.; Lipinskas, T.; Galinis, A.; Miksys, D.; Maltsev, V.V.; Leonyuk, N.I.; Kuleshov, N.V. Monolithic 1.5 μm Er,Yb:$GdAl_3(BO_3)_4$ eye-safe laser. *Opt. Mat.* **2019**, *88*, 60–66. [CrossRef]
13. Cheng, W.; Zhang, T.; Jiang, Z.; Huang, G.; Huang, Y.; Li, B.; Lin, Z.; Chen, Y.; Huang, Y.; Lin, Y.; et al. 4.55 W continue-wave dual-end pumping of Er:Yb:$YAl_3(BO_3)_4$ microchip laser at 1.5 μm. *Appl. Phys. Lett.* **2023**, *123*, 171101. [CrossRef]
14. Chen, Y.; Lin, Y.; Huang, J.; Gong, X.; Luo, Z.; Huang, Y. Fabrication and diode-pumped 1.55 μm continuous-wave laser performance of a diffusion-bonded Er:Yb:$YAl_3(BO3)_4$/$YAl_3(BO_3)_4$ composite crystal. *Opt. Express* **2017**, *25*, 17128–17133. [CrossRef]
15. Gorbachenya, K.N.; Kisel, V.E.; Deineka, R.V.; Yasukevich, A.S.; Kuleshov, N.V.; Maltsev, V.V.; Mitina, D.D.; Volkova, E.A.; Leonyuk, N.I. Continuous-wave laser on Er,Yb-codopedpentaborate crystal. *Devices Methods Meas.* **2019**, *10*, 301–307. [CrossRef]
16. Huang, Y.; Yuan, F.; Sun, S.; Lin, Z.; Zhang, L. Thermal, spectral and laser properties of Er^{3+},Yb^{3+}:$GdMgB_5O10$: A new crystal for 1.5 μm lasers. *Materials* **2018**, *11*, 25. [CrossRef]
17. Huang, Y.; Sun, S.; Yuan, F.; Zhang, L.; Lin, Z. Spectroscopic properties and continuous-wave laser operation of Er^{3+},Yb^{3+}:$LaMgB_5O_{10}$ crystal. *J. Alloy Compd.* **2017**, *695*, 215–220. [CrossRef]
18. Chen, Y.; Hou, Q.; Huang, Y.; Lin, Y.; Huang, J.; Gong, X.; Luo, Z.; Lin, Z.; Huang, Y. Efficient continuous-wave diode-pumped Er^{3+}:Yb^{3+}:$LaMgB_5O_{10}$ laser with sapphire cooling at 1.57 μm. *Opt. Express* **2017**, *25*, 19320–19325. [CrossRef]
19. Chen, Y.; Huang, Y.; Lin, Z.; Huang, Y. Passively Q-switched Er,Yb:$GdMgB_5O_{10}$ pulse laser at 1567 nm. *OSA Contin.* **2019**, *2*, 3598–3603. [CrossRef]
20. Huang, Y.; Lou, F.; Sun, S.; Yuan, F.; Zhang, L.; Lin, Z.; You, Z. Spectroscopy and laser performance of Yb^{3+}:$GdMgB_5O_{10}$ crystal. *J. Lumines* **2017**, *188*, 7–11. [CrossRef]
21. Gorbachenya, K.N.; Yasukevich, A.S.; Lazarchuk, A.I.; Kisel, V.E.; Kuleshov, N.V.; Volkova, E.A.; Maltsev, V.V.; Koporulina, E.V.; Yapaskurt, V.O.; Kuzmin, N.N.; et al. Growth and Spectroscopy of Yb:$YMgB_5O_{10}$ Crystal. *Crystals* **2022**, *12*, 986. [CrossRef]
22. Sun, S.; Wei, Q.; Li, B.; Shi, X.; Yuan, F.; Lou, F.; Zhang, L.; Lin, Z.; Zhong, D.; Huang, Y.; et al. The $YMgB_5O_{10}$ crystal preparation and attractive multi-wavelength emission characteristics of doping Nd^{3+} ions. *J. Mater. Chem. C* **2021**, *9*, 1945–1957. [CrossRef]
23. Wang l Liu, S.; Gou, H.; Chen, Y.; Yue, G.H.; Peng, D.L.; Hihara, T.; Sumiyama, K. Preparation and characterization of the ZnO:Al/$Fe_{65}Co_{35}$/ZnO:Al multifunctional films. *Appl. Phys. A Mater. Sci. Process.* **2011**, *106*, 717–723. [CrossRef]
24. Maltsev, V.V.; Mitina, D.D.; Belokoneva, E.L.; Volkova, E.A.; Koporulina, E.V.; Jiliaeva, A.I. Synthesis and flux-growth of rare-earth magnesium pentaborate crystals $RMgB_5O_{10}$ (*R* = Y, Gd, La, Tm and Yb). *J. Cryst. Growth* **2022**, *587*, 126628. [CrossRef]
25. Petricek, V.; Dusek, M.; Palatinus, L. Crystallographic computing system JANA2006: General features. *Z. Krist.* **2014**, *229*, 345–352. [CrossRef]
26. Putz, H.; Brandenburg, K. *Match!—Phase Analysis Using Powder Diffraction, Crystal Impact*; GbR: Bonn, Germany. Available online: https://www.crystalimpact.de/match (accessed on 16 July 2024).
27. *Inorganic Crystal Structure Data Base—ICSD*; Fachinformations Zentrum (FIZ) Karlsruhe: Karlsruhe, Germany, 2021. Available online: https://www.crystallography.net/cod/ (accessed on 16 July 2024).
28. Zhang, J.; Tao, X.; Cai, G.; Jin, Z. Phase relation, structure, and properties of borate $MgYB_5O_{10}$ in MgO–$Y2O_3$–B_2O_3 system. *Powder Diffr.* **2017**, *32*, 97–106. [CrossRef]
29. Burns, P.; Dawes, J.; Dekker, P.; Pipper, J.; Jiang, H.; Wang, J. Optimization of Er,Yb:YCOB for cw laser operation. *IEEE J. Quantum Electron.* **2004**, *40*, 1575–1582. [CrossRef]
30. Sumida, D.S.; Fan, T.Y. Effect of radiation trapping on fluorescence lifetime and emission cross section measurements in solid-state laser media. *Opt. Lett.* **1994**, *19*, 1343–1345. [CrossRef]
31. Yasyukevich, A.S.; Shcherbitskii, V.G.; Kisel, V.E.; Mandrik, A.V.; Kuleshov, N.V. Integral method of reciprocity in the spectroscopy of laser crystals with impurity centers. *J. Appl. Spectr.* **2004**, *71*, 202–208. [CrossRef]